SMC-TR-00-39

AEROSPACE REPORT NO.
TR-99(8570)-2

Multiple Discrete-Energy Ion Features in the Inner Magnetosphere: Polar Observations

20 December 1998

Prepared by

J. F. FENNELL, M. W. CHEN, and J. L. ROEDER
Space and Environment Technology Center
Technology Operations

W. K. PETERSON and K. J. TRATTNER
Lockheed Martin Space Sciences Laboratory
Palo Alto, CA

R. FRIEDEL and S. LIVI
Max-Planck-Institut für Aeronomie
Katlenburg-Lindau, Germany

M. GRANDE and C. PERRY
Rutherford Appleton Laboratory
Chilton, Didcot, Oxon, U.K.

T. A. FRITZ and R. SHELDON
Boston University
Boston, MA

Prepared for

SPACE AND MISSILE SYSTEMS CENTER
AIR FORCE MATERIEL COMMAND
2430 E. El Segundo Boulevard
Los Angeles Air Force Base, CA 90245

Engineering and Technology Group

THE AEROSPACE CORPORATION
El Segundo, California

REPORT DOCUMENTATION PAGE

Form Approved
OMB No. 0704-0188

1. AGENCY USE ONLY (*Leave blank*)	2. REPORT DATE	3. REPORT TYPE AND DATES COVERED
	20 December 1998	

4. TITLE AND SUBTITLE
Multiple Discrete-Energy Ion Features in the Inner Magnetosphere: Polar Observations

5. FUNDING NUMBERS
F04701-93-C-0094

6. AUTHOR(S)
J. F. Fennell, M. W. Chen, J. L. Roeder, W. K. Peterson, K. J. Trattner, R. Friedel, S. Livi, M. Grande, C. Perry, T. A. Fritz, and R. Sheldon

7. PERFORMING ORGANIZATION NAME(S) AND ADDRESS(ES)
The Aerospace Corporation
Technology Operations
El Segundo, CA 90245-4691

8. PERFORMING ORGANIZATION REPORT NUMBER
TR-99(8570)-2

9. SPONSORING/MONITORING AGENCY NAME(S) AND ADDRESS(ES)
Space and Missile Systems Center
Air Force Materiel Command
2430 E. El Segundo Boulevard
Los Angeles Air Force Base, CA 90245

10. SPONSORING/MONITORING AGENCY REPORT NUMBER
SMC-TR-00-39

11. SUPPLEMENTARY NOTES

12a. DISTRIBUTION/AVAILABILITY STATEMENT
Approved for public release; distribution unlimited

12b. DISTRIBUTION CODE

13. ABSTRACT (*Maximum 200 words*)
The Polar satellite traverses the inner magnetosphere twice in 18 h. On many traversals of the inner magnetosphere, multiple-peaked spectra are observed by the ion composition sensors (CAMMICE/MICS and TIMAS) with peaks in the energy ranges near 2–5, 10–20, 35–50, and 90–120 keV as Polar moves from high L to cross the equator near L = 2.5–3.5. The multi-peaked spectra are observed most often on the dayside (6–18 MLT), and the peaks appear as traces that extend from large to small L values. They are similar to classic "nose" events except for the multiplicity of discrete energy peaks or "traces" that extend over a wide L range. For example, on February 9, 1998, the MICS observed such traces extending from L = 7 to 3.5 that had at least 5 discrete energy peaks in H^+ near 3.5, 18, 32, 65, and 90 keV/q at L = 3.5. The three lowest energy peaks were also observed in He and O^+. These were well below the ~L^{-3} trace corresponding to the peak energy of the quiet time ring current, which had a broad spectral peak in the H^+ near 400 keV at L ~ 3.5. These discrete energy traces may be consistent with the motion of ions inward from the magnetotail during a period that had a fluctuating cross polar cap electric field. However, standard particle tracing in combined model electric and magnetic fields can only explain some but not all these discrete energy traces. The lowest energy ion features appear to correspond to "banana" type closed drift shells near the Earth as predicted by standard particle trajectory calculations.

14. SUBJECT TERMS
Polar satellite, magnetosphere

15. NUMBER OF PAGES
6

16. PRICE CODE

17. SECURITY CLASSIFICATION OF REPORT	18. SECURITY CLASSIFICATION OF THIS PAGE	19. SECURITY CLASSIFICATION OF ABSTRACT	20. LIMITATION OF ABSTRACT
UNCLASSIFIED	UNCLASSIFIED	UNCLASSIFIED	

Acknowledgment

We want to thank R. Lepping and K. Ogilvie for allowing the use of the WIND data. The effort at Aerospace was supported in part under subcontract GC 131165 to Boston University and Air Force contract FP47P1-91PC-0089. The work at Boston University was supported in part by Aerospace subcontract 46-00000260 and NASA grant NAG-30368. The CAMMICE effort at Max-Planck-Institute for Aeronomy was supported by DARA grants 50OC89131, 50OC95022, and 50OC89110. The work at Lockhed was supported by NASA contract NAS5-30302, and the HYDRA effort in the U.S. was supported under NASA grant NAG5-2231.

1. Introduction

The energetic ions observed at geocentric distances from near geosynchronous orbit to 4 RE (i.e. on McIlwain L shells from <7 to 4) near the equator have been extensively studied (e.g. *McIlwain*, 1972, *Smith and Hoffman*, 1974, *Ejiri et al.*, 1980, *Kistler et al.*, 1989). Many of the energetic ions in this region are on open drift paths and eventually leave the magnetosphere through the dayside magnetopause. For a given radial distance the separation between open and closed drift paths is relatively well defined. Ions on the open drift paths do not generally become part of the permanent ring current but represent a 'partial' ring current which has a classic 'nose' (*Smith and Hoffman*, 1974) signature. The properties of these ion distributions in conjunction with sophisticated modeling have been used to investigate the Earth's convection electric field (*McIlwain*, 1972) and to test models of magnetosphere convection. Most of the observations of ions on L shells inside of geosynchronous orbit have been made from satellites in equatorial orbits. Observations from polar orbiting satellites (e.g. *Shirai et al.* 1997; *Kistler et al.* 1998) have been made at lower altitudes significantly removed from the equator where charge exchange and off-equatorial effects complicate the use of ion spectra to infer large scale magnetospheric configuration or dynamics.

The Polar satellite has observed many instances of 'nose' events but here we focus on the occurrence of very narrow, in energy, convection features, especially those that show multiple discrete energy structures extending to very low L's. We will examine in detail a Polar traversal of the post-noon magnetosphere and show the ion convection signatures observed over a wide range of energies on L shells < 6 and compare the results with expectations. We will also provide some preliminary statistics on the occurrence of such events in the Polar data including those that show only a single discrete energy feature in addition to the normal ring current energy profile.

2. Instrumentation

NASA's Polar satellite was launched into a 2×9 R_E orbit with 86° inclination in February 1996. Polar carried a full complement of particle instruments. More importantly, Polar sampled the equatorial region near ~2.5 R_E and high latitudes to ~9 R_E geocentric. The instrumentation used for this study provides complete mass resolved ion

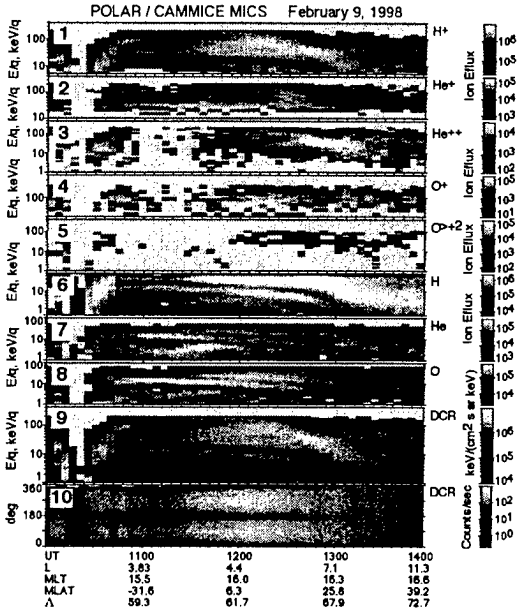

Figure 1. MICS ion spectrogram for 1000-1400 UT on February 9, 1998. Each panel is labeled with the ion type plotted. DCR is a MICS total-ion channel. The ion energy flux is plotted in panels 1-9 according to the gray-scale bars. Panel 10 shows the DCR angular distribution integrated over the energy range 1-220 keV/q.

spectra over the range from thermal to 220 keV/q. Here we use data from the CAMMICE/ MICS (*Wilken et al.*, 1992), TIMAS (*Shelley, et al.*, 1995.) and HYDRA (*Scudder, et al*, 1995) sensors on POLAR. The MICS sensor measures the fluxes, angular distributions and charge states of the major ions (H^+, He^+, He^{++}, $O^{<+3}$, $O^{>+3}$) in the energy range from ~1 to 220 keV/q. TIMAS measures the fluxes and angular distributions of these major ions in the energy range from 15 to 32000 eV/q. HYDRA measures the electron and total-ion fluxes and angular distributions for energies from 10 to 20000 eV/q. Such measurements allowed us to observe complicated signatures of magnetosphere convection that may be used to infer characteristics of the temporal and spatial properties of ions in the plasma sheet and outer plasmasphere.

3. Observations

The February 9, 1998 convection feature event is typical of many such events observed on Polar, such as the September 3, 1997 event discussed by *Peterson et al.* (1998). Figure 1 shows a multi-panel summary of the February 9, 1998 event from the MICS perspective. The ion energy fluxes [keV/(cm^2 s sr keV)] are coded as indicated by the gray-scale bars to the right of each panel. The lowest energy measurements made by MICS are only on a mass per charge basis (see panels 6-8). The energy fluxes of He^{++} (panel 3), He^+ (panel 2) and $O^{<3+}$ (panel 4) are measured for energies >2, >18 and >40 keV/q respectively. As is obvious from Fig. 1, there were few He^{++}, He^+ and O^+ ions above these MICS thresholds. This is borne out by TIMAS data (not shown) which observed weak fluxes of these ions, below the MICS sensitivity level for energies > 1 keV/q. Panel 10 of Fig. 1 shows the MICS total-ion angular distribution integrated over the energy range 1-220 keV/q and provides a sense of the gross angular distributions of the ions plus an indication of the pitch angle coverage of the MICS data.

During the period of interest, Polar was in the 15-16 MLT region of the inner magnetosphere . Polar was in the near earth plasma sheet and ring current from ~1025-1505 UT. The minimum L value obtained was L~3.5 at 1125 UT near 15.7 MLT. During Polar's traversal of the inner magnetosphere, spectra with multiple energy peaks were observed in the MICS, TIMAS, and HYDRA data. These appear in Fig. 1 as distinct bright traces in the energy-time domain (e.g. Fig. 1 panel 9). The Polar traversal spanned the inner magnetosphere twice from L>12 down to L~3.5 first at high southern magnetic latitudes and low altitudes (-77°<MLAT<-18°; 1.98<R<3.45 R_E) then northward at higher altitudes and somewhat lower magnetic latitudes (-18°<MLAT<39°; 3.45<R<6.8 R_E) near 13-17 MLT.

Close examination of Fig. 1 shows that there are multiple discrete energy features in these spectrograms in the interval 1045-1300 UT and that these are seen in all the major ions. These are particularly clear in panels 1, 2, 6, 7, 8 and 9. Panel 10 of Fig. 1 shows the angular distribution of the >1 keV/q ions which, for the most part, had trapped distributions during the period of interest. However, near 1300 UT there was a short interval where a separate field aligned population was observed. Near 1100 UT MICS only sampled to within 20° of the field line direction. These angular distributions will be compared with the TIMAS data below.

Fig. 1 shows that all the ions had the same discrete energy peaks and that these peaks or 'traces' are continuous in L and observed down to ~3 keV/q (see panel 9) in the MICS data. These same traces, plus others, were observed in the TIMAS and HYDRA data (not shown). In particular, the low energy TIMAS and HYDRA data showed there was significant structure in the <1 keV/q ion fluxes. (The HYDRA data were separated into parallel, perpendicular, and anti-parallel to **B** fluxes). The energy structure was

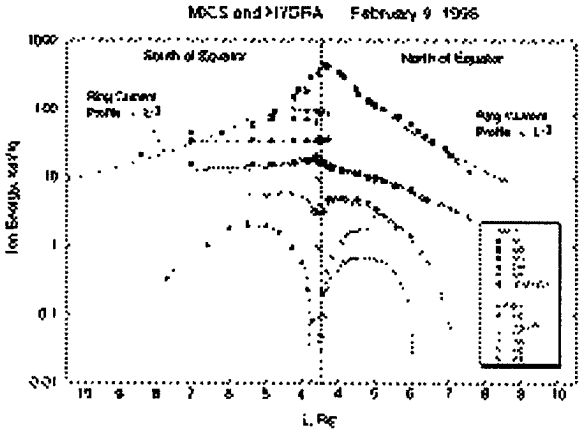

Figure 2. Radial profile of the energy peaks from Fig. 1 and from the HYDRA data (not shown). The symbols labeled Mx are from MICS and those labeled Hx are from HYDRA. Data from CEPPAD/IPS were used to complete the ring current radial profile at the highest energies.

most clear in the HYDRA fluxes antiparallel to **B** and least clear in the perpendicular fluxes. This was consistent with the TIMAS ion angular distributions that will be discussed below. There were also discrete energy features or traces like those of Fig. 1 in the HYDRA electron data but they will not be discussed here.

We extracted the energies of the spectral peaks for all the traces from all three data sets and have replotted those from MICS and HYDRA as peak-energy versus L in Figure 2 (Mx symbols are from MICS and Hx symbols from HYDRA data). The normal ring current energy versus L profile, as extracted from the MICS and CEPPAD IPS (*Blake et al.*, 1995) data, is also shown in Fig. 2 (top curve). Each trace is identified separately in the legend. The solid and open symbols making up a single trace indicate when data from both instruments were used to construct the profile (e.g. points M2 and H5). The M1 and H4 traces in Fig. 2 can be compared to the lowest energy traces in Fig. 1 panels 7 and 8 for He and O. The low energy He and O ions clearly match the H4 trace of Fig. 2 which was obtained from the HYDRA data. The M2 and H5 from Fig. 2 match the higher energy He and O traces in Fig. 1 panels 7 and 8. M2 and H5 also matched the TIMAS H^+, O^+ and He^+ traces (not shown). Thus, three (four with IPS) independent measurements gave the same discrete energy structures and they also indicated that these traces existed for all the major ion species.

The agreement between the MICS and HYDRA data in the energy overlap regions gives confidence that the discrete energy peaks are real and not instrumental effects. We used these E vs. L profiles in our modeling calculations described below. As Fig. 2 shows, the ring current profiles had a nominal L^{-3} dependence. All the other peak energy traces were at energies below the ring current peak with some having peak energies that were essentially independent of L (see curves M2, H5, M3, and M4) south of the equator. Other traces had minimum energy near the equator at L~3.5 with the peak energy maximizing near L=4.5-5.5. The M1 and H4 curves in Fig. 2 correspond to the lowest energy trace in Fig. 1 (Note: in Fig. 2 the H2_UB is the upper bound energy of a separate low energy plasma population and it is not clear whether H1 and H3 are the same population or not.)

Figure 3 shows the TIMAS angular distributions for H^+ and O^+ separated into two different energy groups, <5

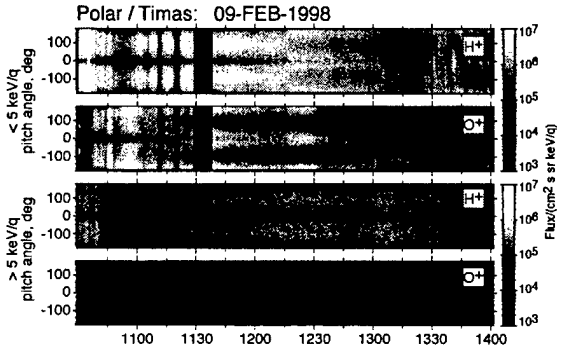

Figure 3. TIMAS H^+ and O^+ angular distributions for 1030-1400 UT on February 9, 1998. Top two panels are for ions < 5 keV/q and bottom two panels are for ion > 5 keV/q.

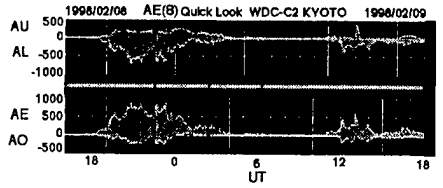

Figure 4. AE for February 8-9, 1998.

keV/q and > 5 keV/q. The pitch angles cover the range 0-360°, representing a complete Polar satellite rotation. The >5 keV/q ions were peaked perpendicular to **B** throughout the period of interest while the <5 keV/q ions had long intervals where the ions were field aligned. In particular, the O^+ ions were predominantly field aligned and relatively intense during the 1040-1310 UT interval. The H^+ were predominantly field aligned in the 1215-1310 UT interval. Both were field aligned from 1320-1400 UT. This is to be compared to the MICS >1 keV/q ions which were field aligned only for a short time near 1300 UT (Fig. 1 panel 10). The combination of Fig. 1 and Fig. 3 plus the HYDRA data (not shown) indicate that the field aligned ions were mostly low energy, below the MICS threshold of 1 keV/q. The TIMAS energy-time spectrograms (not shown here) indicated there was a relatively (intense) flux of <600 eV H^+ and O^+ ions present from ~1035-1325 UT. The HYDRA data (also not shown) placed the inner edge of the plasma sheet electrons (<1 keV) at 1330 UT. Thus, the field aligned ions may be the high energy tail of the plasmaspheric population or may correspond to a refilling of the plasmasphere following the substorm activity from late on February 8, 1998.

Figure 4 shows the quick look AE for the period of interest. There was significant substorm activity late on February 8 followed by a long period of relative quiet prior to the Polar observations starting near 1030 UT. There was some moderate activity from 1200-1400 UT during the period when Polar was outbound in the northern hemisphere. The WIND interplanetary magnetic field and the solar wind plasma data plus the DMSP plasma convection data (*Anderson*, 1998) showed that both the solar wind and cross polar cap electric fields varied significantly just prior to and during the period of Polar's traversal through the inner magnetosphere. For example, the IMF turned southward near 0900 UT on February 9, 1998. At the end of 8 February the solar wind electric field had been relatively strong for about 6 hours (B_Z<-1.5 nT with minimum ~ −2.7 nT) and this continued into February 9 until about 0100 UT. At that time the B_Z turned northward until about 0830 UT when it turned southward modestly. The B_Z>0 period coincides with the period of low and zero AE in Figure 4. The IMF B_Z changes are also reflected in the estimates of the cross-tail potentials shown in Figure 5. The combination of an extended period of northward IMF (weak solar wind electric field coupling to the magnetosphere) and the corresponding inactivity at all auroral latitudes preceding the Polar observations provides a quiet initial condition for what ensued after 0830 UT. The weak to moderate magnetospheric electric field that occurred in conjunction with B_Z turning southward at 0830 UT had only ~2 hours to modify the particle trajectories deep in the magnetosphere prior to the observations in Fig. 1. The subsequent

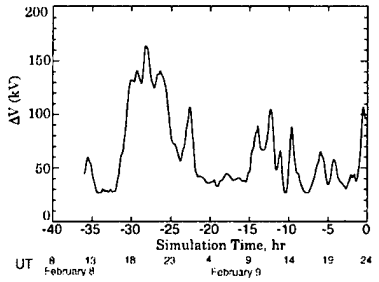

Figure 5. Cross-tail potential used in simulation. Based on hourly averages of the solar wind electric field and empirical fit by *Reiff et al.* (1981) normalized to DMSP polar cap potential drop observations.

fluctuations in the solar wind electric field may have been responsible, in part, for the generation of some of the multiple ion convection signatures. As Fig. 4 and Fig. 5 show, this latter period had relatively weak activity.

The angular distributions of the ions can be used to provide an indication of the source of the ions in the discrete energy-time traces, especially at low energies. The detailed angular distributions taken by MICS at several energies were trapped or nearly isotropic with at most a narrow loss cone. Thus, ions with >1 keV/q appeared to be trapped, with no obvious local ionospheric source, and they persisted in the face of charge exchange losses. As was shown in Fig. 3, TIMAS observed much the same angular distributions for energies > 5 keV/q. There are hints that the > 5 keV/q O^+, He^+ and He^{++} angular distributions were nearly isotropic around 1215 UT while the H^+ had a normal trapping distribution with relatively empty loss cones. This may indicate that the O^+ and He^+ ions were more recently injected or that they were being more efficiently scattered in pitch angle.

Fig. 3 shows that the <5 keV/q H^+ ions had normal trapped angular distributions except for some intervals beyond ~1215 UT. The O^+ and He^+ (not shown) had field aligned angular distributions starting near 1110 UT for O^+ and near 1140 UT for He^+. The He^+ did have partially filled loss cones starting from 1110 UT. The He^{++} had a highly trapped distribution much like the H^+ in the 1115-1140 UT interval. After 1147 UT the <5 keV/q He^{++} had a weak field aligned component and became essentially only field aligned by 1155 UT. The H^+ ions became field aligned starting near 1215 UT simultaneous with an intensification of the field aligned O^+. O^+ was dominantly field aligned from ~1115 to 1400 UT. The O^+ was most intense for pitch angles in the 150-180° range (see Fig. 3). As Polar proceeded to high L the field aligned low energy ions persisted until ~1300 UT. At later times they are sporadic. Bursts of field aligned H^+, O^+ and He^+ were observed on the inner edge of the plasma sheet, which Polar entered near 1325 UT. The O^+ and He^+, showed that the field aligned ions at the inner edge of the plasma sheet are not symmetric relative to the field direction. Ion fluxes were higher near 130-180° pitch angle than near 0-50°, after 1325 UT. H^+ showed some preference for a field aligned distribution favoring the 150-180° pitch angles after 1325 UT. He^{++} was essentially at background beyond 1305 UT.

What can we infer from the angular distributions? The energies of the field-aligned distributions correspond to

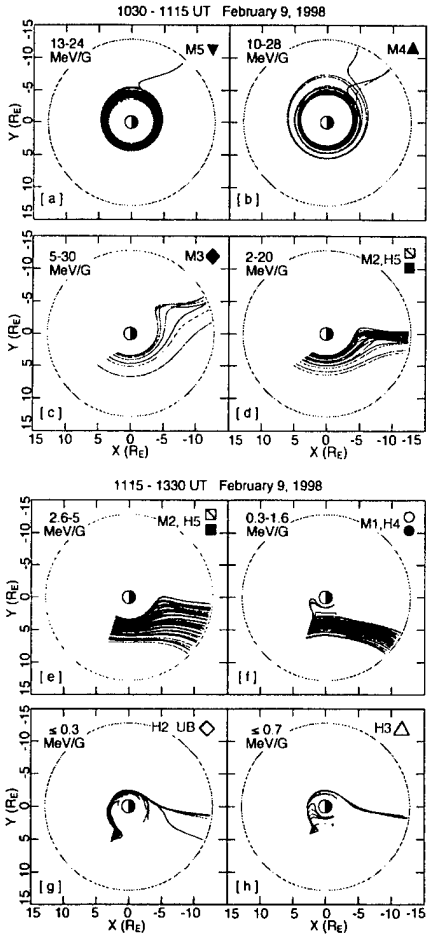

Figure 6. Calculations of H+ trajectories in model electric and magnetic fields for ions measured south (panels a-d) and north (panels e-h) of the magnetic equator. The symbols refer to Fig. 2. The range of first invariant covered by the observations are indicated. The outer boundary circle is at 12 R_E.

curves H3 and H2_UB in Figure 2. Thus, we argue that these features were most likely generated by the field aligned ions, especially the O^+, He^+ and He^{++} ions. We note that the low energy HYDRA features were most clear for the anti-field-aligned direction consistent with the TIMAS observations. The fact that these field aligned distributions favor ~180° when Polar was in the northern hemisphere would argue for upflow from the northern ionosphere towards the equator. Near the equator (~1115-1130 UT) the ions were more perpendicular to **B**. This may indicate there was strong heating or scattering occurring perpendicular-to-**B** as the ions approached the equator.

4. Modeling

We used the empirical relationship of *Reiff et al.* (1981) to relate the solar wind electric field to the cross tail potential and derived the results of Fig. 5. There we show the cross-tail potential drop which has been normalized to available DMSP cross polar cap potential estimates (*Anderson*, 1998) for February 8-9, 1998. The bottom-

most X-axis labeling shows the date and time while the black labeling shows our simulation time. Fig. 5 shows that the expected cross-tail potential was low between ~2 and 9 hours on Feb. 9, 1998 in agreement with Fig. 4. (We used 35 kV as the quiet time value of the potential drop.) In an attempt to understand how the discrete energy traces in Figs. 1 and 2 could have arisen, we have traced H^+ ion trajectories backwards in time from their observation point to see where they may have originated. The ions were traced according to a scheme described in *Chen et al.* (1993). The cross-tail potential shown in Fig. 5 was used in the calculations. The trajectory results are shown in Figure 6. Each panel corresponds to a single trace in Fig. 2 and is labeled using the plot symbol and legend labels from Fig. 2. The ion trajectories were started at the observation points along the polar trajectory. They were traced backwards in time until they either crossed the circular boundary at L~12 or had traveled for 24 hours. As can be seen in Figs 6a and 6b, the higher energy particles are predicted to be on or close to closed drift shells. A slight increase in the cross-tail potential drop would probably put all the trajectories in Figs. 6a and 6b on open drift shells.

Fig. 6b and 6e-6h show that the higher energy ions come from the post-midnight regions and the lower energy ions from the pre-midnight region. Figure 7 shows trajectories for quiet time cross tail potentials and four different first invariant values. These can be compared to the trajectories in Fig. 6. The lowest energy ions (Figs. 6g and 6h) are nearly stagnant with some trajectories on closed drift shells very close to the earth much like Figs. 7b and 7c. Fig. 7b shows the so called 'banana orbits' which are similar to features seen in the trajectories of Fig. 6f-6h. These latter trajectories correspond to the <5 keV/q ions that were field aligned in Fig. 3. This argues that these ions may have a local source such as the ionosphere, since ions external to the near earth regions with similar first invariant values normally cannot access these near earth closed drift shells.

While we have determined the drift times for H+ in the model, we do not have the space here to present those detailed results. Suffice it to say that the transport times relative to the substorm time (ref. Fig. 4) are consistent with some, but not all of the observations. Transport time alone

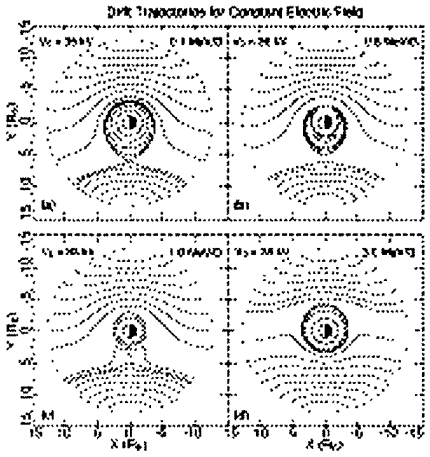

Figure 7. Quiet time trajectories for ions of selected first invariant values.

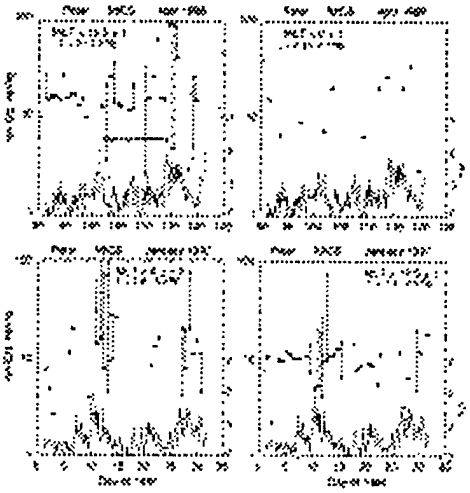

Figure 8. Sample statistics for convection features observed by Polar/MICS in noon-midnight and dawn-dusk planes for 30 day intervals. K_p is at the bottom of each panel

is unable to account for the multiple energy peaks observed independent of whether the source regions are the distant plasma sheet or a near geosynchronous injection boundary.

5. Statistics of convection features

We have gathered some preliminary statistics on the occurrence of the discrete energy features or traces. We required that there be at least one trace and that it extend from high (L>5) to low L and that it be observed as Polar crossed the magnetic equator. The traces were always in addition to and occurred at energies below the peak of the quite-time ring current. The peak energy of each observed trace was determined at the magnetic equator. Some examples of the results are shown in Figure 8 where the energy of the observed spectral peaks are plotted as a function of time. Each panel represents a thirty day interval centered at the MLT indicated. The L range of the equatorial crossing point is also noted. The multiple spectral peaks or traces from a given Polar orbit are connected by a vertical line. K_p is plotted at the bottom of each panel (RH axis label) for reference. A summary of the statistics for a seven month period is given in Table 1. As Fig. 8 and Table 1 show, the occurrence of spectral peaks or traces is greatest on the dayside and least near midnight. For example, the dusk and noon occurrence of at least one trace was 80% and 60%, respectively. Generally, multiple traces occurred in association with enhanced magnetic activity or during the recovery

Table 1. Traces at Magnetic Equator

MLT Sector	%Orbits with traces	%Orbits with multipe traces
noon	60	20
pre noon	21	10
post noon	51	7
dawn	54	21
dusk	80	15
pre midnight	41	5
midnight	30	2
post midnight	21	10

from such activity. Table 1 also shows the percentage of orbits that had multiple traces. Again, the occurrence peaks on the dayside of the magnetosphere , especially in the noon and dawn-dusk sectors.

6. Discussion

Similar ion signatures have been observed in the inner magnetosphere in the past. The classic nose events discussed by *Smith and Hoffman* (1974), *Kistler et al.*, (1989) and *Sheldon et al.* (1998) are one class of such events. In fact, *Sheldon et al.* (1998) describes energetic ion traces that are similar in energy to the M3 and M5 traces of Fig. 2. We find the > 1 keV/q ions in these energetic features have angular distributions peaked perpendicular to **B** whereas Sheldon et al. (1998) argues that the ions are field aligned and that they were accelerated to ~ 40 keV locally. Unfortunately, the MICS and TIMAS instruments were turned off during the *Sheldon et al.* (1998) event and could not confirm the angular distributions nor provide the ion composition.

For the February 9, 1998 event some ion features may be consistent with the picture shown in *Peterson et al.* (1998; their Fig. 3) with the difference that some of the present observations argue for a source relatively close to earth (3 R_E<R<geosynchronous altitude). This close-in source corresponds to the region of field aligned low energy ions observed by TIMAS in Fig. 3. The ionosphere is the likely source of these ions based on the significant fluxes of < 1 keV/q O^+ and He^+. What is confusing, is why field aligned H^+ was not present at all times with field aligned O^+ and He^+. This we do not understand yet. If the low energy field aligned ion composition is ionospheric then we would expect to observed significant fluxes of field aligned H^+ too. There may be mass dependent acceleration processes occurring which favors the heavier ions over H^+, such as the ion cyclotron acceleration thought to generate conic ion distributions at low altitudes in the auroral zone or wave processes which are thought to heat the plasmaspheric 'cloak' (see *Lin et al.*, 1992 and *Singh and Horwitz*, 1992 and references therein). This requires further study.

A second source for the ions observed on February 9, 1998 is the near-to-distant plasma sheet. Such ions can come from deep in the tail or from a region such as the injection boundary (*Mauk and Meng*, 1987). Along the satellite trajectory, ions from both sources can co-exist. The only difference is how and when they arrive at the satellite. For the more distant source, the different energy ions take different paths. The multiple peaks in the ion distributions can be partially explained by the time dependent transport. The different energy ions take different times/paths to reach Polar and ions in the adjacent energy intervals, the missing ions, either have not arrived by the time of the satellite passage or their drift trajectories take so long that they have been lost to charge exchange prior to reaching Polar. Since the convection features are identical for all the major species, the drift times and source(s) for the > 1 keV/q ions are not mass dependent. That is, all species simultaneously had the same features at the same energies. However, as noted above, the calculated drift times cannot explain all the traces. We may have to search for electric field configurations which are consistent with the observed ion traces, much as was done by *McIlwain* (1972), or use more accurate models .

In summary, we have presented an example of multiple ion-energy features in the inner magnetosphere. For energies >1 keV/q these features appear to be partially but not completely consistent with a standard picture of convection inward from the plasma sheet under the influence of the cross magnetosphere electric field with the twist of time dependent electric fields and time-of-flight effects thrown in. For energies <1 keV/q the ions appear to be from a more local source as evidenced by the field aligned angular distributions which could not be sustained in the presence of charge exchange losses unless ions are continuously being accelerated. The position of our observations of these low energy ions is consistent with their playing a role in plasmasphere refilling. In the future we will be tracing > 1 keV ions in combined magnetic and time dependent data driven electric field models to see if we can put constraints on the source regions for each of the ion features.

Acknowledgments. We want to thank R. Lepping and K. Ogilvie for allowing the use of the WIND data. The effort at Aerospace was supported in part under subcontract GC 131165 to Boston University and Air Force contract FP47P1-91PC-0089. The work at Boston University was supported in part by Aerospace subcontract 46-00000260. and NASA grant NAG5-30368. The CAMMICE effort at Max-Planck-Institute for Aeronomy was supported by DARA grants 50OC89131, 50OC95022 and 50OC89110. The work at Lockheed was supported by NASA contract NAS5-30302, and the HYDRA effort in the U.S. was supported under NASA grant NAG 5 2231.

References

Anderson, P. C.,, private communication, 1998.
Ejiri, I. et al., *J. Geophys. Res.* ***85***, 653, 1980.
Blake, J. B., et al., *Space Sci. Rev.*, ***71***, 531, 1995.
Chen, J. et al., *Geophys. Res. Lett.*, ***24***, 1447, 1997.
Chen, M. W., et al., *J. Geophys. Res.*, ***98***, 3835, 1993.
Kistler, L. M. et al., *J. Geophys. Res.*, ***94***, 3579, 1989.
Kistler et al., *Geophys. Res. Lett.*, in press, 1998.
Lin et al., *J. Geophys. Res.*, ***99***, 5727, 1994.
McIlwain, C. E., in *Earth's Magnetospheric Processes*, B. M. McCormac ed., p268, Reidel Pub., 1972.
Mauk, B., and C. -I. Meng, *Physica Scripta,* ***T18***, 128, 1987.
Olsen, R. C., *J. Geophys. Res.*, ***97***, 1135, 1992.
Peterson, W. K., et al., *Proceedings of the International Substorm Conference,* Terra Scientific, Tokyo, 1998.
Reiff, P. H., et al., *J. Geophys. Res.*, **86**, 7639, 1981.
Scudder, et al., *Space Sci. Rev.*, ***71***, 459-495, 1995.
Singh, N., and J. Horwitz, *J. Geophys. Res.*, ***97***, 1049, 1992.
Shelley, E.G. et al., *Space Sci. Rev.*, ***71***, 1995.
Sheldon, R. B., et al., *Geophys. Res. Lett.*, **10**, 1617, 1998.
Shirai, et al., J. Geophys. Res. **102**, 19873, 1997.
Smith, P. and R. Hoffman, *J. Geophys. Res.*, ***79***, 966, 1974.
Wilken, B., et al., *J. Spacecraft and Rockets,* ***29***, 585 (1992)

LABORATORY OPERATIONS

The Aerospace Corporation functions as an "architect-engineer" for national security programs, specializing in advanced military space systems. The Corporation's Laboratory Operations supports the effective and timely development and operation of national security systems through scientific research and the application of advanced technology. Vital to the success of the Corporation is the technical staff's wide-ranging expertise and its ability to stay abreast of new technological developments and program support issues associated with rapidly evolving space systems. Contributing capabilities are provided by these individual organizations:

Electronics and Photonics Laboratory: Microelectronics, VLSI reliability, failure analysis, solid-state device physics, compound semiconductors, radiation effects, infrared and CCD detector devices, data storage and display technologies; lasers and electro-optics, solid state laser design, micro-optics, optical communications, and fiber optic sensors; atomic frequency standards, applied laser spectroscopy, laser chemistry, atmospheric propagation and beam control, LIDAR/LADAR remote sensing; solar cell and array testing and evaluation, battery electrochemistry, battery testing and evaluation.

Space Materials Laboratory: Evaluation and characterizations of new materials and processing techniques: metals, alloys, ceramics, polymers, thin films, and composites; development of advanced deposition processes; nondestructive evaluation, component failure analysis and reliability; structural mechanics, fracture mechanics, and stress corrosion; analysis and evaluation of materials at cryogenic and elevated temperatures; launch vehicle fluid mechanics, heat transfer and flight dynamics; aerothermodynamics; chemical and electric propulsion; environmental chemistry; combustion processes; space environment effects on materials, hardening and vulnerability assessment; contamination, thermal and structural control; lubrication and surface phenomena.

Space Science Application Laboratory: Magnetospheric, auroral and cosmic ray physics, wave-particle interactions, magnetospheric plasma waves; atmospheric and ionospheric physics, density and composition of the upper atmosphere, remote sensing using atmospheric radiation; solar physics, infrared astronomy, infrared signature analysis; infrared surveillance, imaging, remote sensing, and hyperspectral imaging; effects of solar activity, magnetic storms and nuclear explosions on the Earth's atmosphere, ionosphere and magnetosphere; effects of electromagnetic and particulate radiations on space systems; space instrumentation, design fabrication and test; environmental chemistry, trace detection; atmospheric chemical reactions, atmospheric optics, light scattering, state-specific chemical reactions and radiative signatures of missile plumes.

Center for Microtechnology: Microelectromechanical systems (MEMS) for space applications; assessment of microtechnology space applications; laser micromachining; laser-surface physical and chemical interactions; micropropulsion; micro- and nanosatellite mission analysis; intelligent microinstruments for monitoring space and launch system environments.

Office of Spectral Applications: Multispectral and hyperspectral sensor development; data analysis and algorithm development; applications of multispectral and hyperspectral imagery to defense, civil space, commercial, and environmental missions.